

Supplementary Information

Boosting the anchoring and catalytic capability of MoS₂ for high-loading lithium sulfur batteries

Zheng-Long Xu,^{a*} Nicolas Onofrio,^{b*} Jian Wang^c

^aDepartment of Industrial and Systems Engineering, The Hong Kong Polytechnic University, Hung Hom, Hong Kong, Email: zhenglong.xu@polyu.edu.hk

^bDepartment of Applied Physics, The Hong Kong Polytechnic University, Hung Hom, Hong Kong, Email: nicolas.onofrio@polyu.edu.hk

^cDepartment of Chemistry, Seoul National University, 1 Gwanak-ro, Gwanak-gu, Seoul 151-742, Republic of Korea

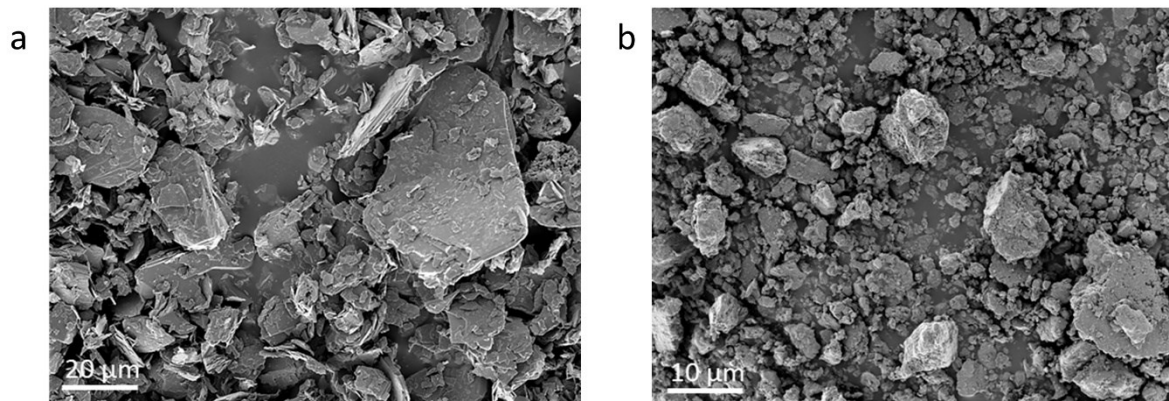


Fig. S1 SEM images of (a) pristine 2H MoS₂, (b) grinded 2H MoS₂. Pristine MoS₂ presents large sizes of about 20 μm, while, the average sizes for grinded sample is about 1 μm.

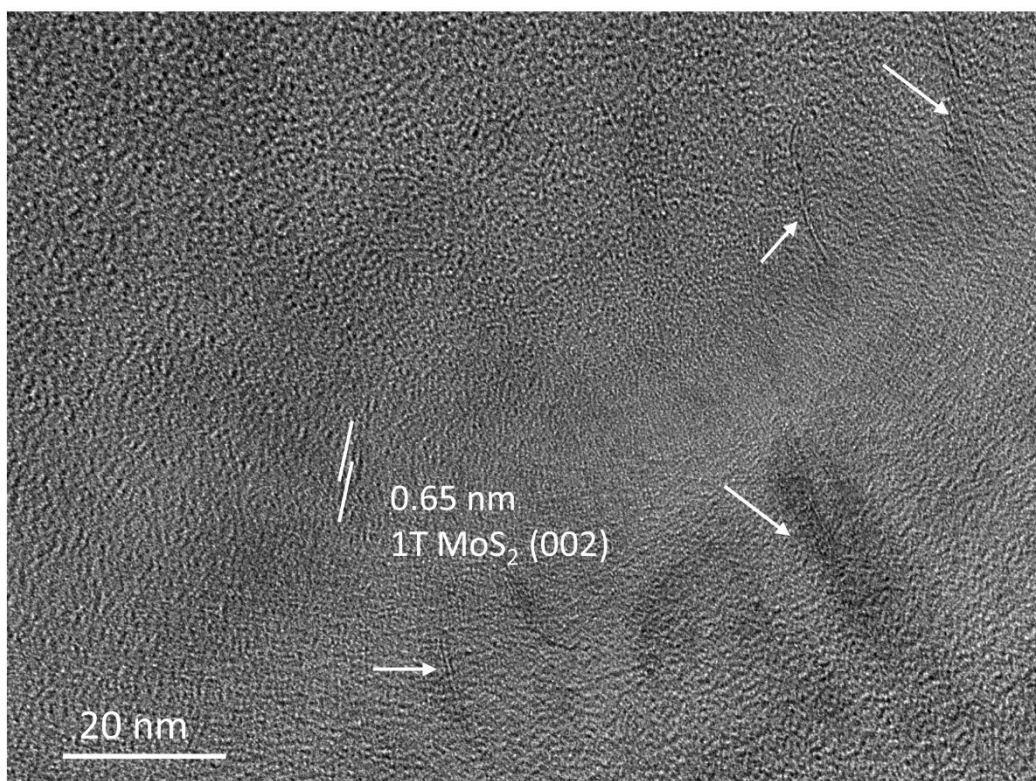


Fig. S2 HRTEM image of 1T MoS₂ NDs. The exfoliated MoS₂ shows a lattice fringe of 0.65 nm, corresponding to the (002) plane. White arrows indicate the very thine MoS₂ NDs.

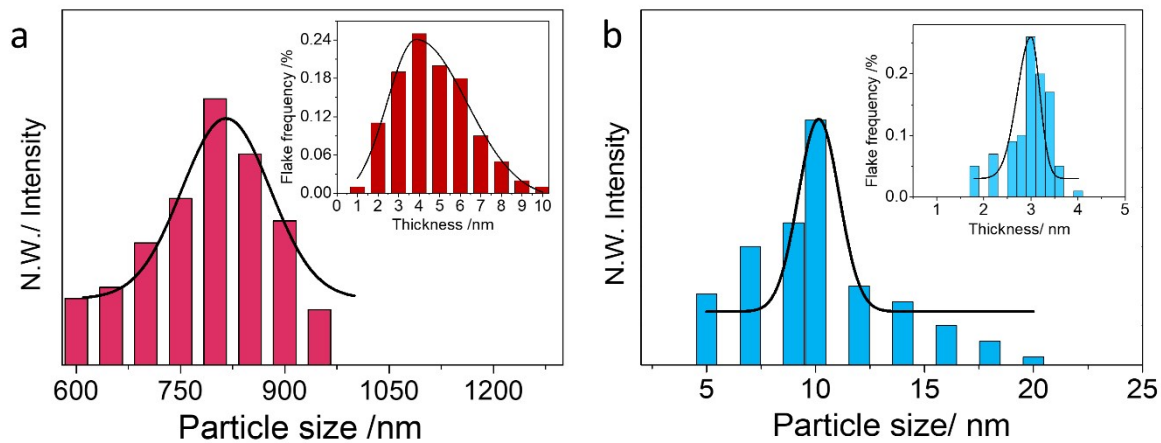


Fig. S3 Dimensions of the MoS₂ flakes characterized by AFM. Particle size/thickness dimensions of (a) MoS₂ sheet and (b) MoS₂ NDs. The statistical results are coinciding with the TEM observations in Figs. 1a and d in main content.

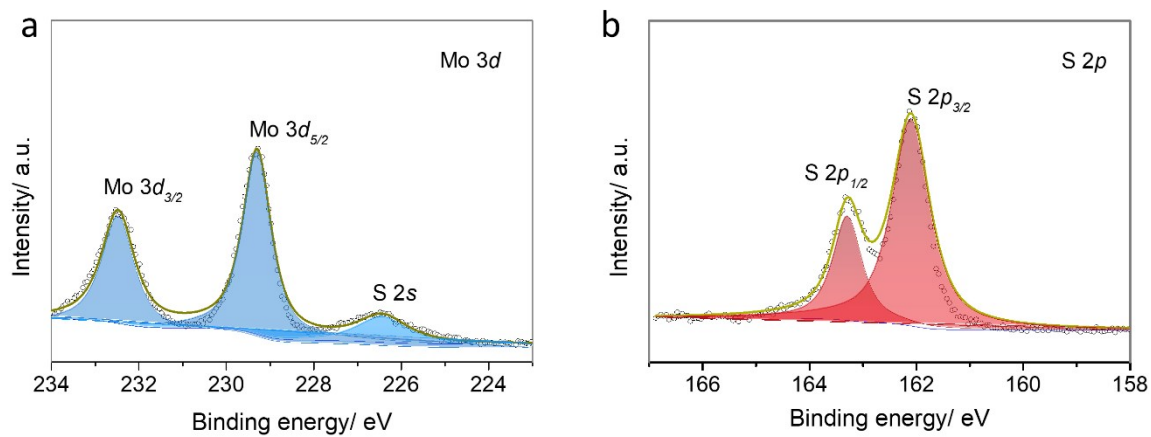


Fig. S4 Deconvoluted (a) Mo 3d and (b) S 2p XPS spectra for bulk 2H MoS₂.

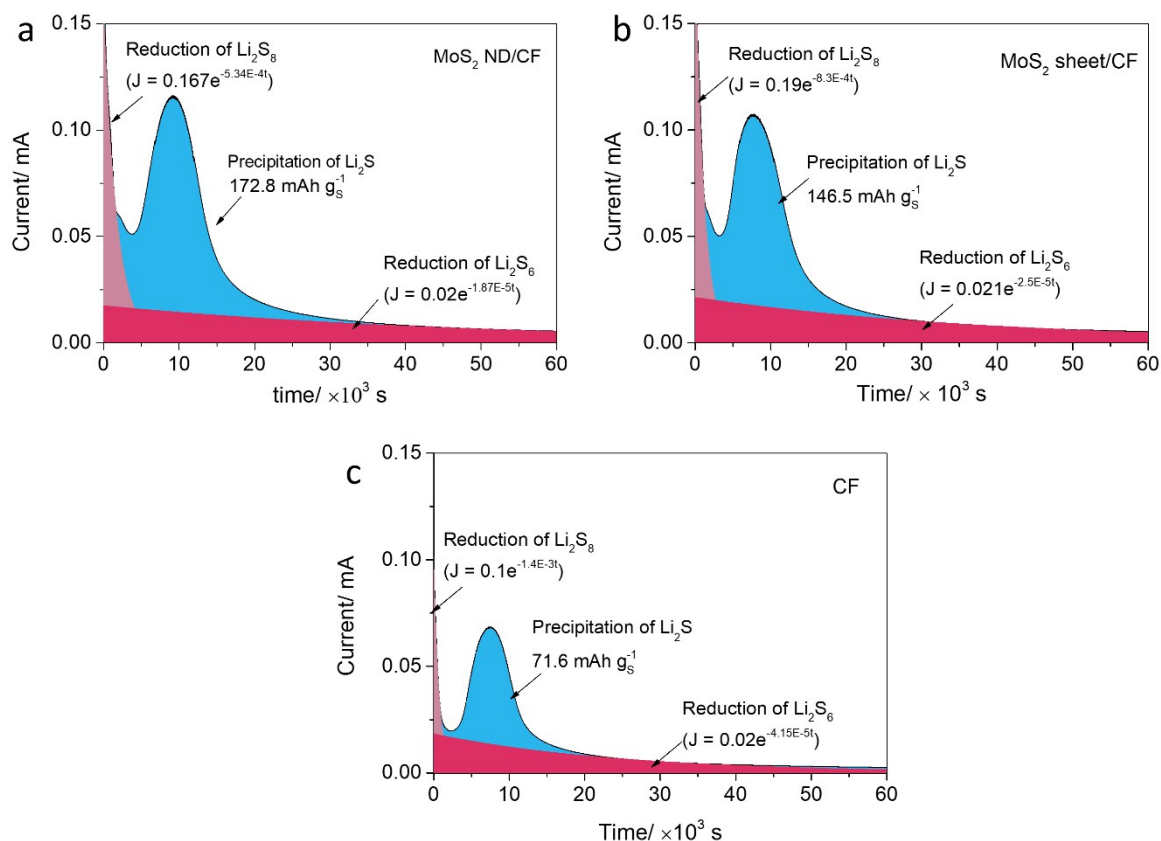


Fig. S5 Fitting of current vs. time for potentiostatic discharge at 2.05V on different surfaces. (a) MoS₂ ND/CF, (b) MoS₂ sheet/CF and (c) CF. The nucleation and growth rates of Li₂S on different substrates were fitted accordingly to Faraday's law. Specifically, the potentiostatic discharge curve at 2.06 V was fitted using the integration of the exponentially decayed curves, representing the reduction of Li₂S₈ and Li₂S₆, respectively. When an overpotential was applied at 2.05V, Li₂S forms, contributing extra value to the overall current. The capacity from Li₂S formation was calculated by subtracting the capacity of Li₂S₈/Li₂S₆ reductions from overall capacities.

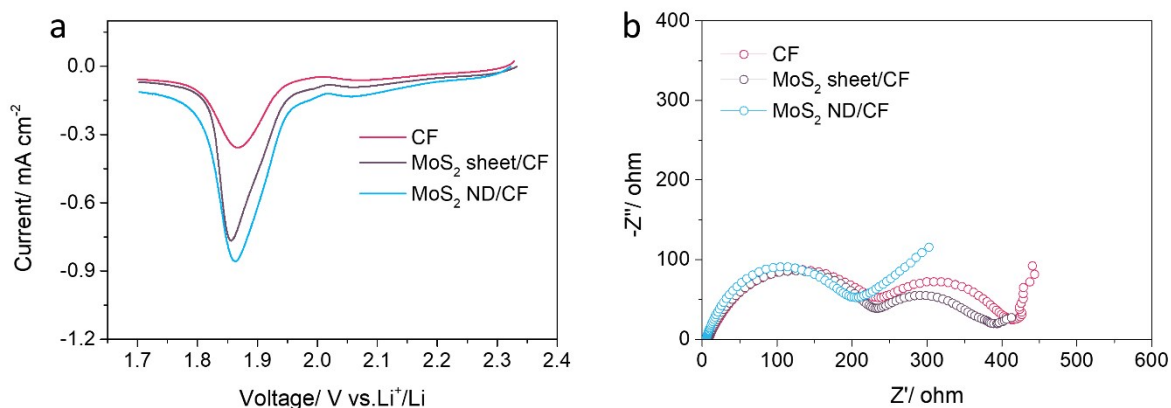


Fig. S6 Linear sweep voltammogram (LSV) and electrochemical impedance spectroscopy (EIS) analyses of CF, MoS₂ sheet/CF and MoS₂ ND/CF electrodes. (a) Forward scan (from OCV to 1.7V) of the three electrodes with Li₂S₄ catholyte. The highest scanning current density of MoS₂ ND/CF than that for CF and MoS₂ sheet/CF electrodes confirms the enhanced reaction kinetics for polysulfide by MoS₂ NDs. (b) Nyquist plots of cells containing these three electrodes and Li metal anodes. MoS₂ ND/CF/Li₂S₄ shows smaller interfacial resistance, possibly due to uniform distribution of ultrasmall MoS₂ ND ameliorating the electrolyte/electrode interfacial impedance.

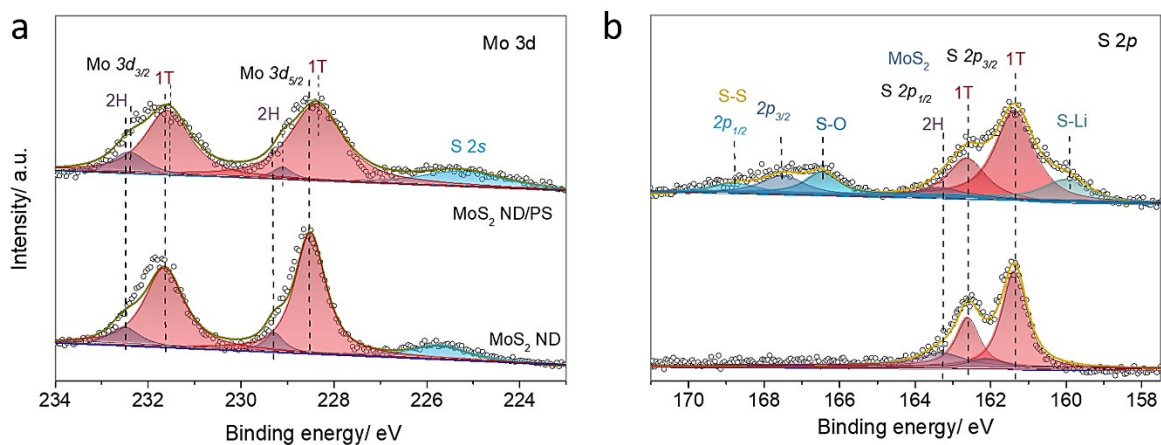


Fig. S7 XPS spectra of (a) Mo 3d and (b) S 2p regions for MoS₂ ND before (down) and after mixing with polysulfides (up). The Mo 3d spectrum for MoS₂ ND could be deconvoluted into four peaks, in which the dominant 231.6 eV and 228.5 eV were corresponding to 1T phase, while the marginal 232.6 eV and 229.3 eV referred to the residual 2H phase. In comparison with original MoS₂ ND, all the four peaks downshifted to lower binding energies after absorbing polysulfides. In S 2p spectra, new peaks at 166.4 eV and 166.4, 167.5 and 168.7 eV were observed for MoS₂ ND/polysulfides. The first new peak corresponds to Li-S interaction between polysulfide and MoS₂, and the last three peaks refer to S-O for thiosulfate and S 2p_{1/2} and 2p_{3/2} for polysulfides.

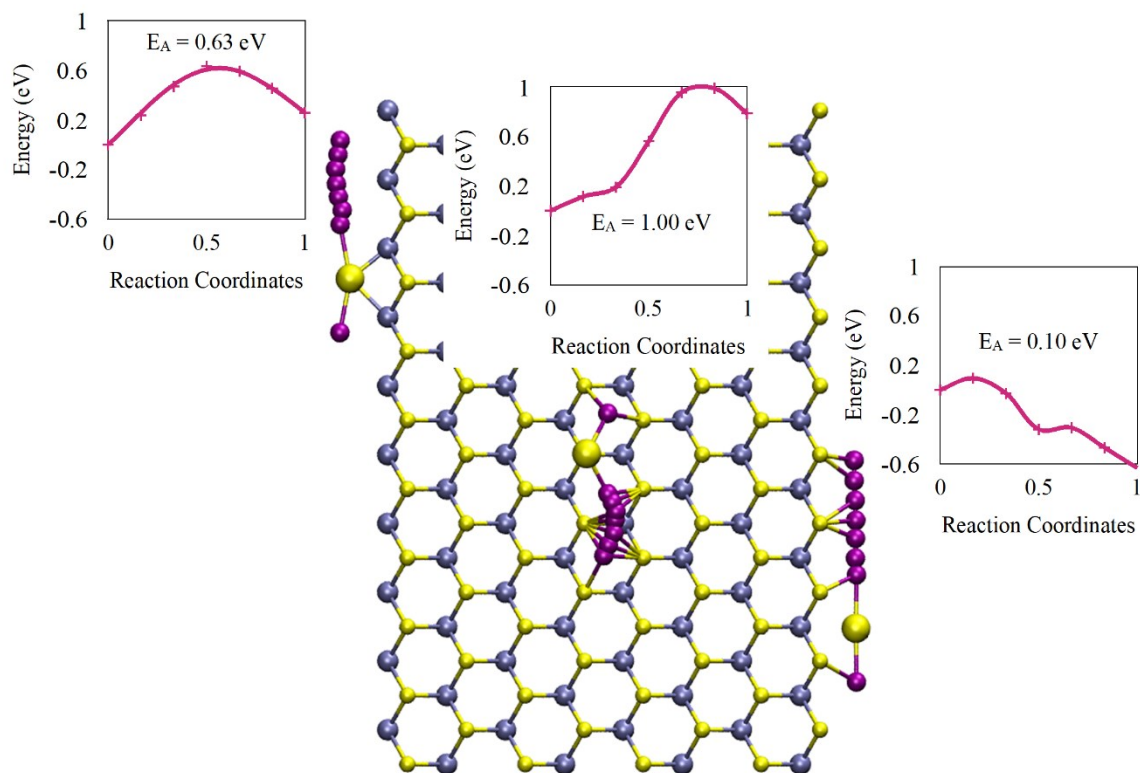


Fig. S8 Molecular structure of the electrochemical dissociation path of Li_2S at various sites on 2H MoS_2 . For each dissociation path, we show the potential energy surface and the corresponding activation energy.

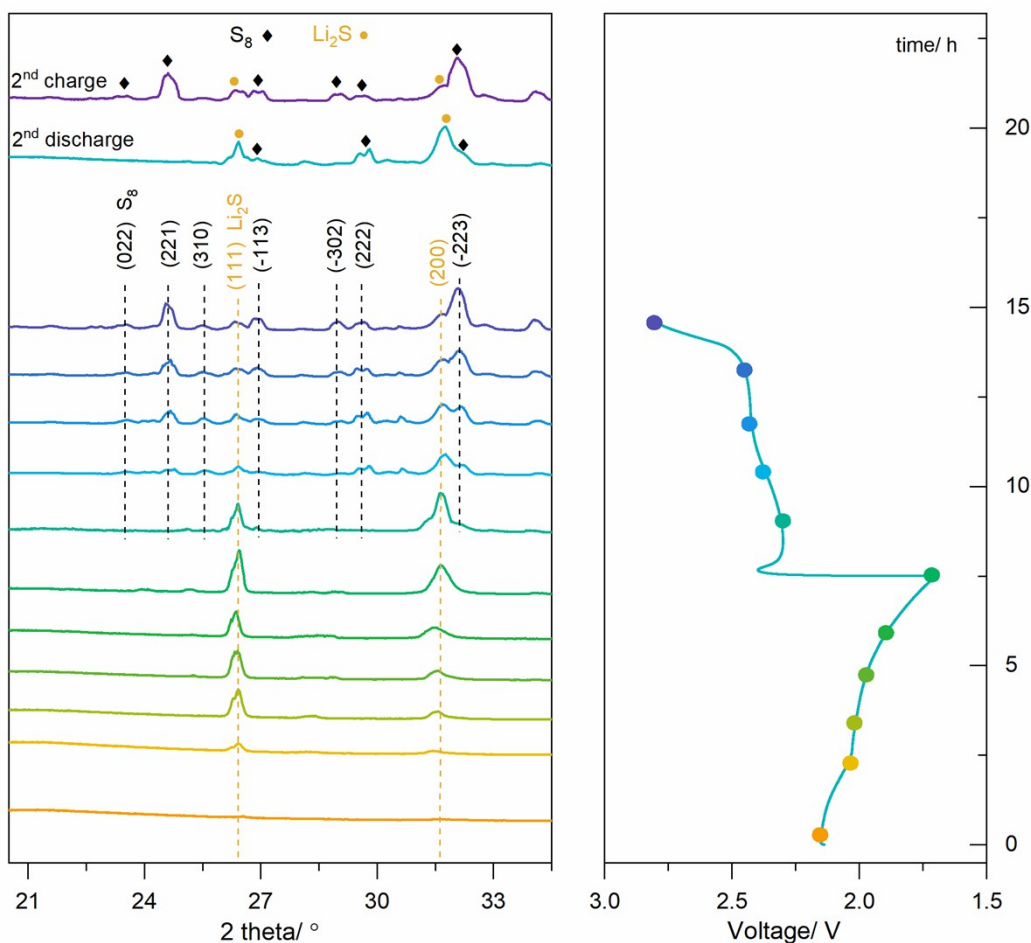


Fig. S9 *In-situ* XRD patterns of conventional 2H MoS₂ flake/porous carbon/Li₂S₆ cathode during 1st cycle. *Ex-situ* XRD patterns of the 2nd discharged and charged electrode were also included on top of the left image. Different from the *in-situ* XRD results of MoS₂ ND/porous carbon/Li₂S₆ in Fig. 4, residual sulfur and Li₂S peaks are observed after full discharging and charging, respectively, suggesting incomplete utilization of active materials during cycles. The *in-situ* XRD characterization was conducted using a Swagelok-type cell on Rigaku Smartlab with Cu-K α radiation source.

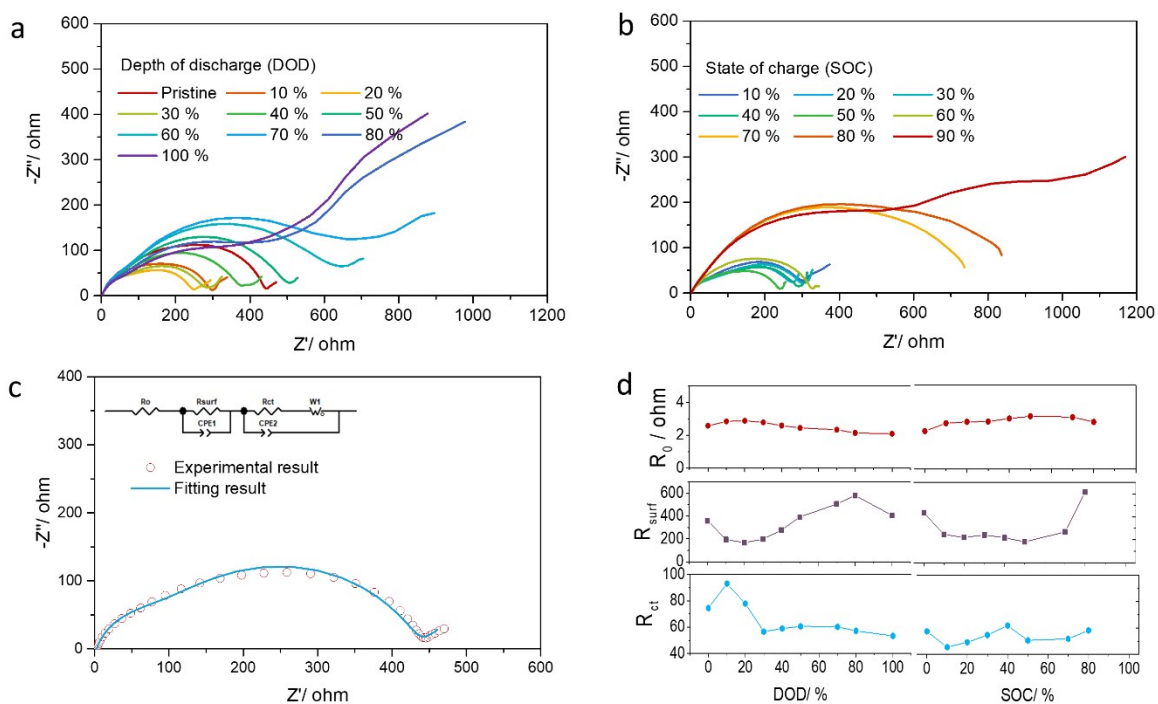


Fig. S10 *In-situ* EIS study of 2nd cycled porous carbon/Li₂S₆ electrodes. (a) Nyquist plots for porous carbon/Li₂S₆ electrode at different DOD. (b) Nyquist plots for porous carbon/Li₂S₆ at different SOC. (c) A typical fitting result of a Nyquist plot of pristine porous carbon/Li₂S₆ electrode. (d) R_s, R_{surf}, R_{ct} obtained from (a) and (b) plotted against DOD or SOC. In (d), R_{ct} decreased from 90 ohm to 55 ohm at the early stage of discharge (DOD = 30%), which may be caused by the component change and enhanced interaction between nonpolar carbon and polar polysulfides during this period, leading to improved charge transfer for polysulfide ions.¹

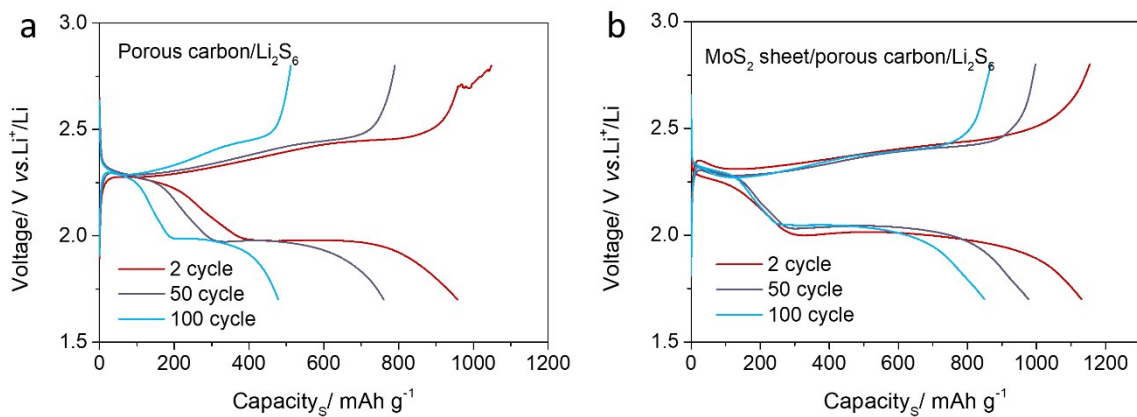


Fig. S11 Discharge/charge voltage profiles for (a) porous carbon/Li₂S₆ and (b) MoS₂ sheet/porous carbon/Li₂S₆ electrodes at 0.1 C. In (a), the charge tail for porous carbon/Li₂S₆ should be attributed to diffusion of polysulfides.

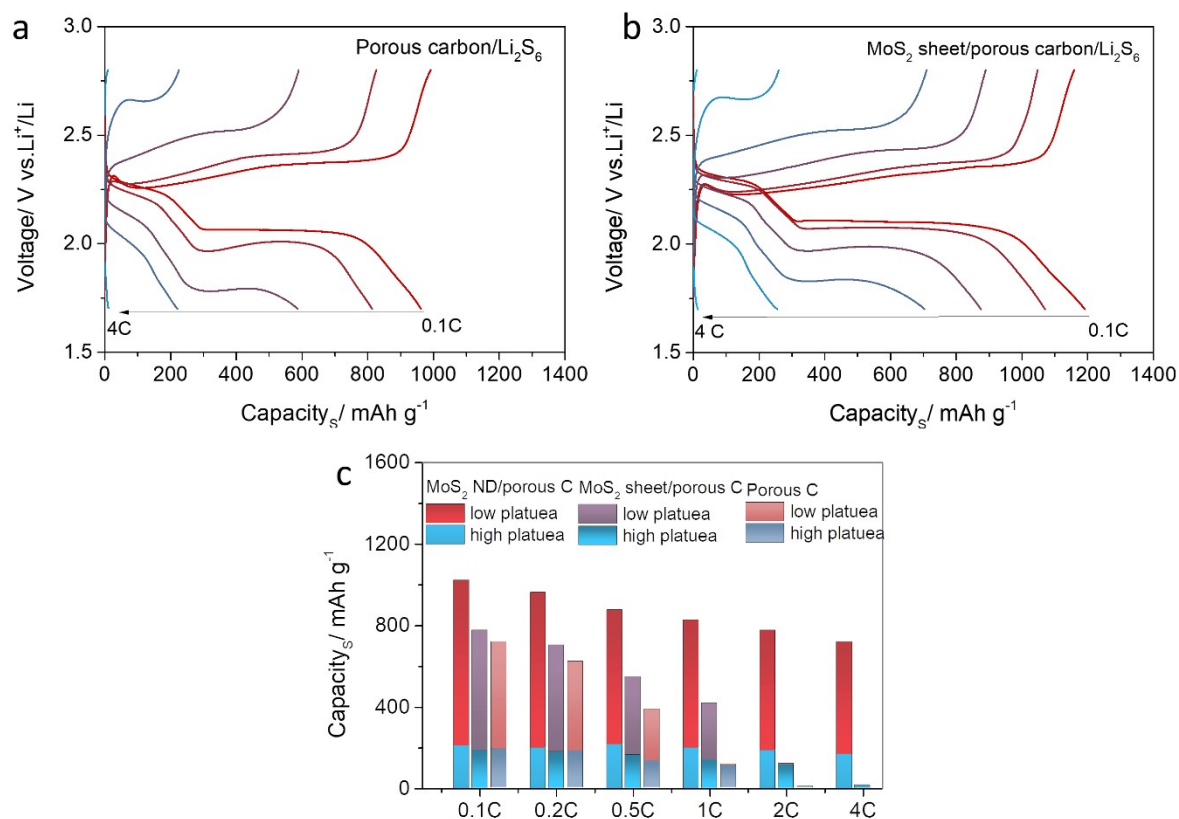


Fig. S12 Rate performance comparison of the porous carbon/Li₂S₆, MoS₂ sheet/porous carbon/Li₂S₆ and MoS₂ ND/porous carbon/Li₂S₆ electrodes. Discharge/charge voltage profiles of (a) porous carbon/Li₂S₆ and (b) MoS₂ sheet/porous carbon/Li₂S₆ electrodes at different C rates. (c) High plateau and low plateau discharge capacities for the three electrodes derived from the rate performance. Due to the diffusion and sluggish redox reaction kinetics for polysulfides, porous carbon/Li₂S₆ and MoS₂ sheet/porous carbon/Li₂S₆ electrodes show negligible discharge capacities at high rates, 2C and 4C, reflecting the superiority of MoS₂ NDs in catalyzing fast Li-S reactions.

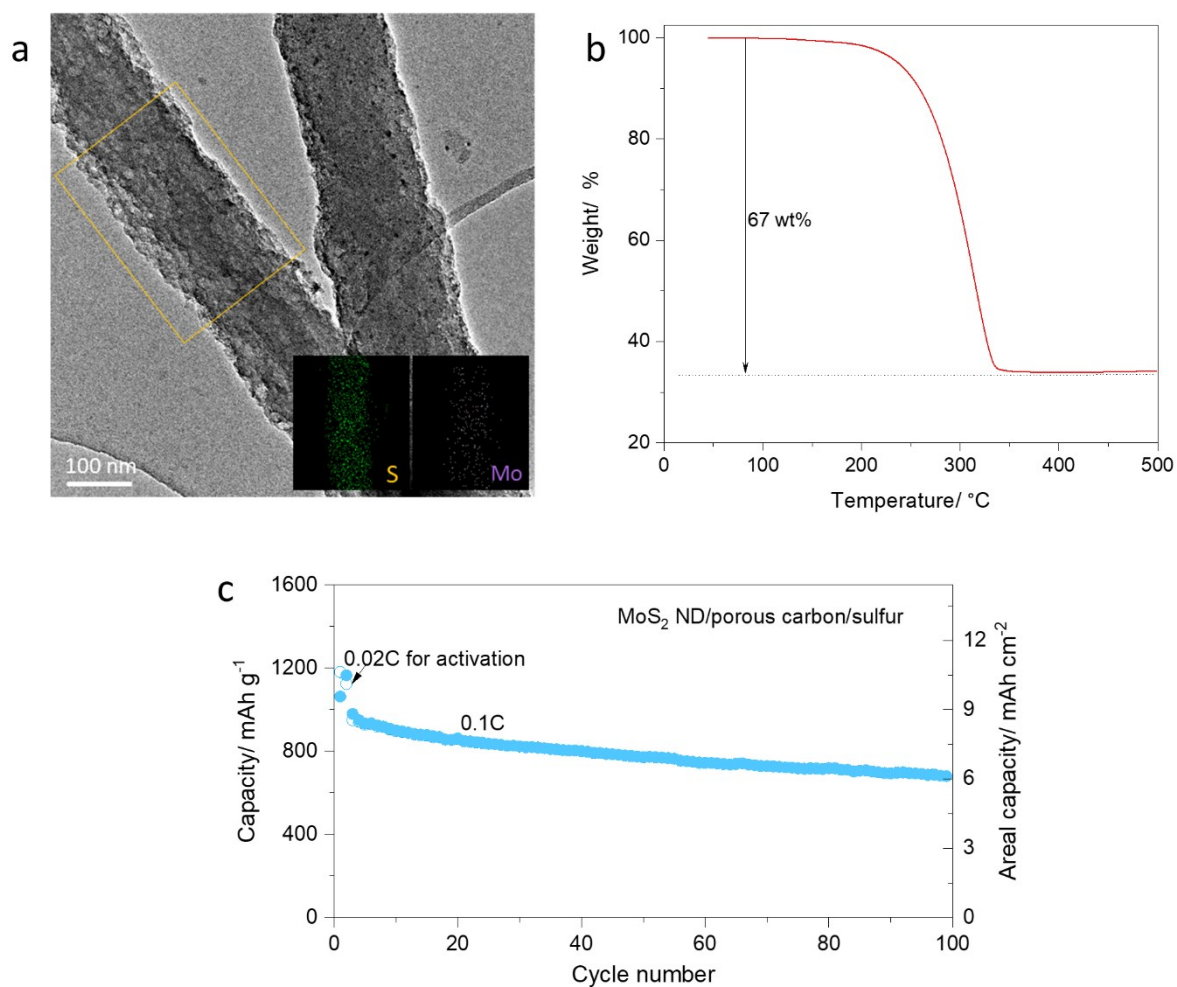


Fig. S13 High loading MoS₂ ND/porous carbon/sulfur cathodes. (a) TEM image of MoS₂ ND/porous carbon/sulfur fibers with successful sulfur impregnation, inset (a) shows uniform distribution of S and Mo elements. (b) TGA curve showing a high sulfur content of 67 wt%. (c) Cyclic capacities of MoS₂ ND/porous carbon/sulfur cathodes under a high sulfur loading of 9 mg cm⁻² and a relatively low E/S ratio of 9.3 μL mg⁻¹. Note that the cyclic capacities are slightly lower than MoS₂ ND/porous carbon/catholyte in the main context, possibly due to the poor immersion of electrolyte in thick sulfur electrodes.

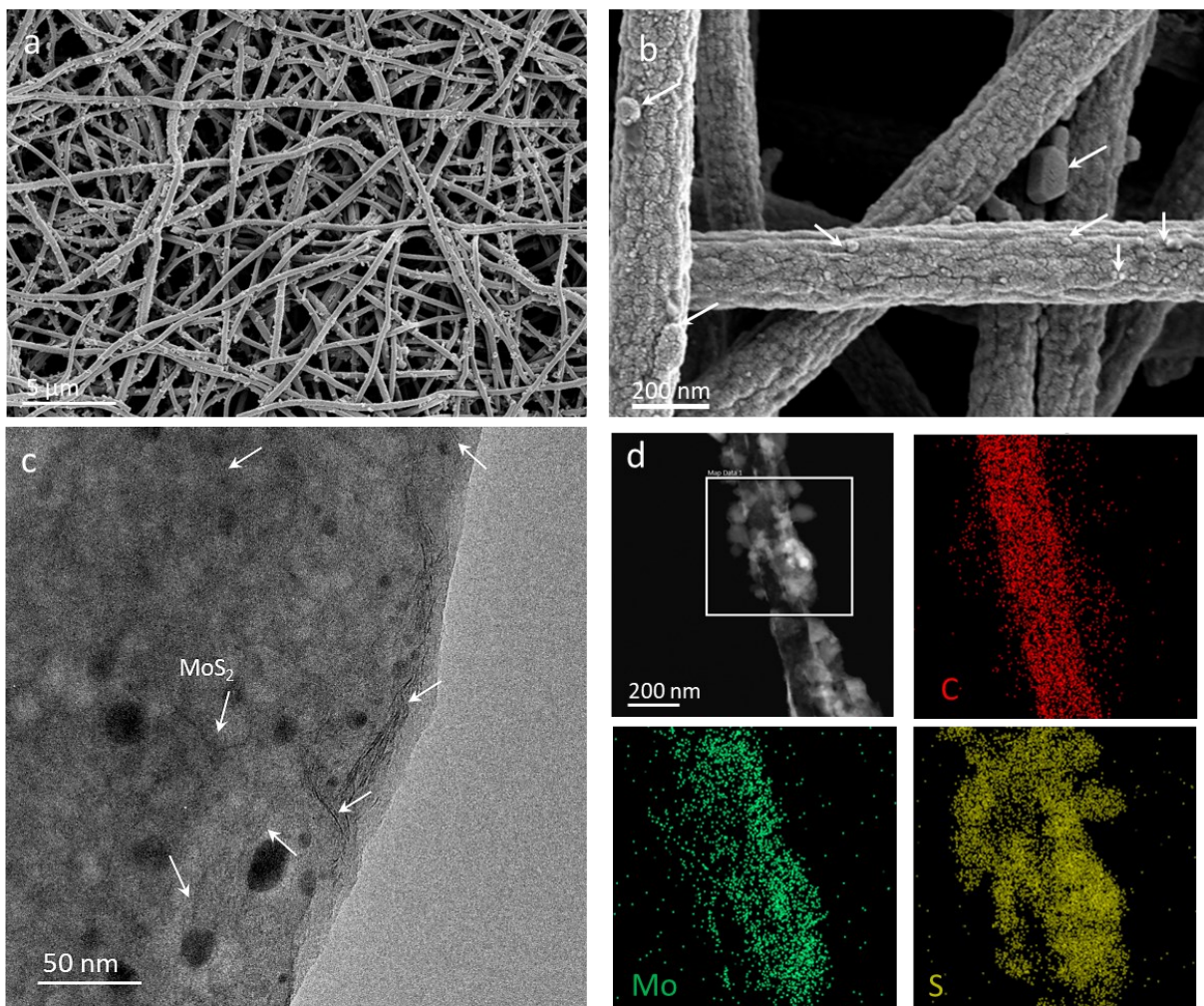


Fig. S14 (a) Low magnification SEM, (b) high magnification SEM, and (c) TEM images of MoS₂ ND/porous carbon, (d) STEM image and C, Mo, S elemental maps of discharged MoS₂ ND/porous carbon/Li₂S₆. White arrows in (b, c) refer to MoS₂. (a-c) clearly illustrates the uniform distribution of MoS₂ ND on porous carbon fiber host. (d) indicates the facilitated Li-S reaction via the evenly dispersed MoS₂ ND catalysts on porous carbon fiber.

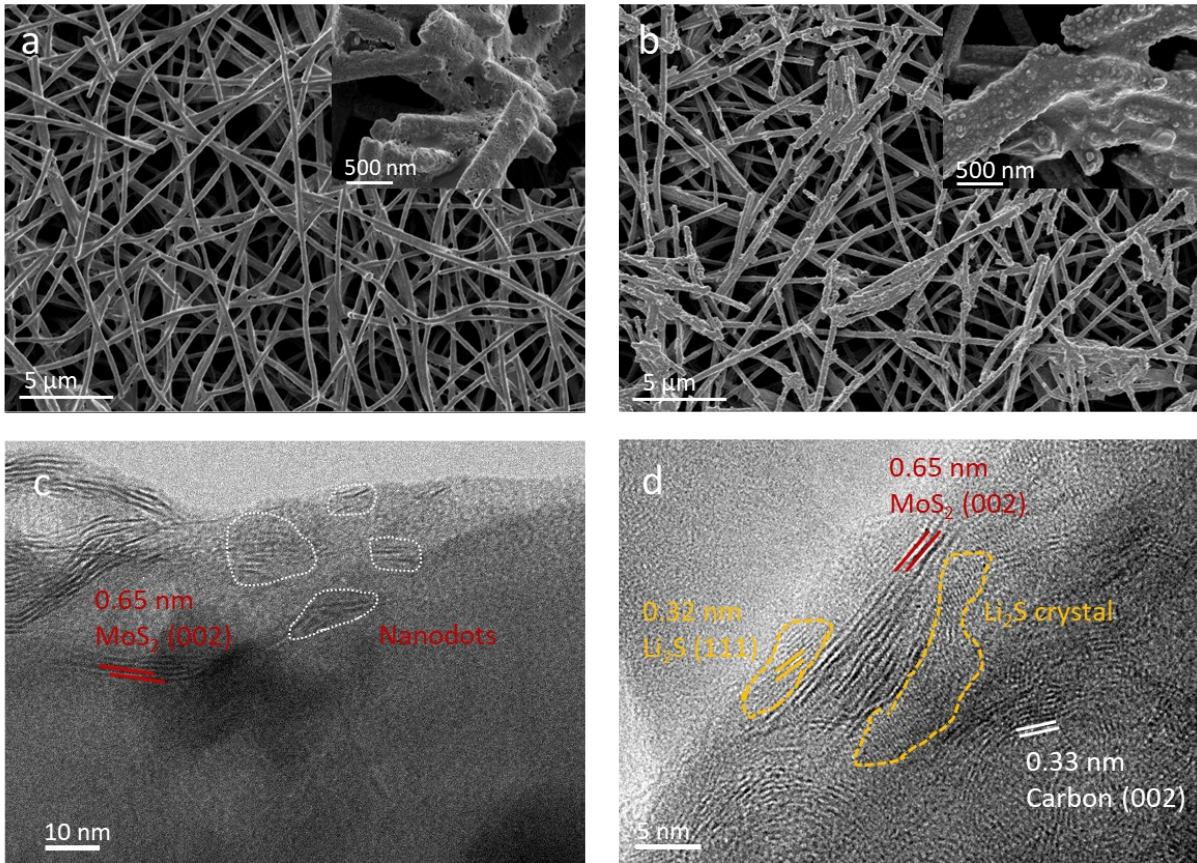


Fig. S15 *Ex-situ* morphological analyses of MoS₂ ND/porous carbon/Li₂S₆ electrode after 100th discharge and charge. SEM images of the electrodes after (a) charging and (b) discharging, HRTEM images for (c) charged and (d) discharged electrode in (a, b). (a) and (b) show that the reaction products sulfur or Li₂S uniformly cover the surface of porous carbon fibers, implying the even dispersion of MoS₂ NDs, promoting the even and fast redox reactions at the electrode/active material interface. In (c) and (d), the MoS₂ nanocrystals are clearly identified, indicating the structural stability for MoS₂ ND catalyst. Li₂S crystals formed on the surface of MoS₂ catalyst in (d) upon discharging.

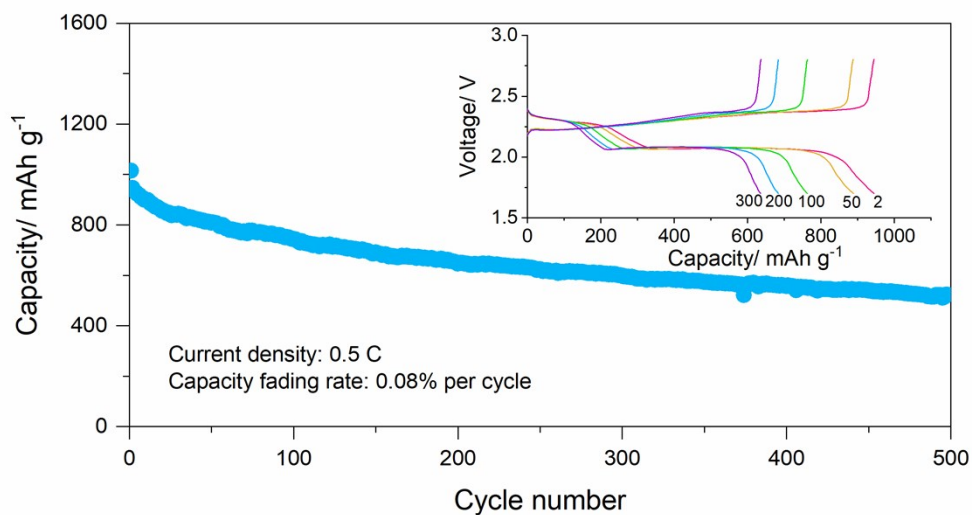


Fig. S16 Cyclic performance of MoS₂ NDs/porous carbon/Li₂S₆ for 500 cycles at 0.5 C. The cells present low capacity fading of 0.08% per cycle and distinctive discharge/charge plateaus inset, both of which evidence the high catalytic capability of MoS₂ NDs during long-term cycling.

Table S1 Binding energies and migration barriers of Li₂S and Li adsorption and Li₂S dissociation on various sites of 1T and 2H MoS₂ (all in eV).

	MoS ₂ phase	Terrace	Mo-edge	S-edge
Li ₂ S adsorption	1T	3.77	6.12	3.30
	2H	1.46	4.98	4.22
Li ₂ S dissociation	1T	0.56	0.52	0.37
	2H	1.00	0.66	0.10
Li adsorption	1T	3.50	3.22	4.13
	2H	1.97	2.31	3.93

Table S2 Comparison of the electrochemical performance of LSBs with different catalysts.

Materials	E/S ratio / $\mu\text{L mg}^{-1}$	Sulfur loading / mg cm^{-2}	Electrochemical performance at high sulfur loading	Reference
Carbon cloth/PS	~8.7	2.32	~1.5 mAh cm^{-2} after 100 cycles	Nat. Energy 2017 ²
VN/graphene/PS	~30	3	~2.7 mAh cm^{-2} after 200 cycles	Nat. Commun.2017 ³
BP sheet/CNF/PS	~10	~5	~6 mAh cm^{-2} after 5 cycles	Adv. Mater. 2017 ⁴
G/Catton carbon/PS	5	46	~20 mAh cm^{-2} after 100 cycles	AM 2018 ⁵
Co/CNT-CNF/PS	6	5.1 9.2	3.9 mAh cm^{-2} after 300 cycles 6.5 mAh cm^{-2} after 50 cycles	EES 2018 ⁶
BPQD/CNF/S	6.5	8	~4.4 mAh cm^{-2} after 200 cycles	Nat. Commun. 2018 ⁷
TiN-TiO ₂ /C/S	6.8	8	~4.3 mAh cm^{-2} after 400 cycles	EES 2019 ⁸
CNT/perovskite particle/S	15	5.2	3.7 mAh cm^{-2} after 100 cycles	AM 2018 ⁹
Mo/CNT/PS	~8	7.6	4.75 mAh cm^{-2} after 100 cycles	ACS Nano 2020 ¹⁰
MoS _{2-x} /rGO/PS	~33	~1.5	~1.2 mAh cm^{-2} after 150 cycles	EES 2017 ¹¹
WS ₂ -WO ₃ /CNT/PS	~10	10	~4.5 mAh cm^{-2} after 250 cycles	AEM2020 ¹²
MoS ₂ ND/porous carbon/PS	~4.6	12.9	~9.4 mAh cm^{-2} after 300 cycles	This work
MoS ₂ ND/porous carbon/S	~9.3	~9	~6.2 mAh cm^{-2} after 100 cycles	This work

Supplementary references

- 1 N. A. Cañas, K. Hirose, B. Pascucci, N. Wagner, K. A. Friedrich and R. Hiesgen, *Electrochim. Acta*, 2013, **97**, 42.
- 2 H. Pan, J. Chen, R. Cao, V. Murugesan, N. N. Rajput, K. S. Han, K. Persson, L. Estevez, M. H. Engelhard, J. G. Zhang, K. T. Mueller, Y. Cui, Y. Shao and J. Liu, *Nat. Energy*, 2017, **2**, 813.
- 3 Z. Sun, J. Zhang, L. Yin, G. Hu, R. Fang, H. M. Cheng and F. Li, *Nat. Commun.*, 2017, **8**, 14627.
- 4 L. Li, L. Chen, S. Mukherjee, J. Gao, H. Sun, Z. Liu, X. Ma, T. Gupta, C. V. Singh, W. Ren, H.-M. Cheng and N. Koratkar, *Adv. Mater.*, 2017, **29**, 1602734.
- 5 S. H. Chung and A. Manthiram, *Adv. Mater.*, 2018, **30**, 1705951.
- 6 G. Li, W. Lei, D. Luo, Y. Deng, Z. Deng, D. Wang, A. Yu and Z. Chen, *Energy Environ. Sci.*, 2018, **11**, 2372.
- 7 Z. L. Xu, S. Lin, N. Onofrio, L. Zhou, F. Shi, W. Lu, K. Kang, Q. Zhang and S. P. Lau, *Nat. Commun.*, 2018, **9**, 4164.
- 8 Z. L. Xu, S. J. Kim, D. Chang, K. Y. Park, K. S. Dae, K. P. Dao, J. M. Yuk and K. Kang, *Energy Environ. Sci.*, 2019, **12**, 3144.
- 9 L. Kong, X. Chen, B. Q. Li, H. J. Peng, J. Q. Huang, J. Xie and Q. Zhang, *Adv. Mater.*, 2018, **30**, 1705219.
- 10 Y. Li, C. Wang, W. Wang, A. Y. S. Eng, M. Wan, L. Fu, E. Mao, G. Li, J. Tang, Z. W. Seh and Y. Sun, *ACS Nano*, 2020, **14**, 1148.
- 11 H. Lin, L. Yang, X. Jiang, G. Li, T. Zhang, Q. Yao, G. W. Zheng and J. Y. Lee, *Energy Environ. Sci.*, 2017, **10**, 1476.
- 12 B. Zhang, C. Luo, Y. Deng, Z. Huang, G. Zhou, W. Lv, Y. He, Y. Wan, F. Kang and Q. Yang, *Adv. Energy Mater.*, 2020, **10**, 2000091.